Photophysical Effects behind the Efficiency of Hot Electron Injection in Plasmon-Assisted Catalysis: The Joint Role of Morphology and Composition

Yoel Negrín-Montecelo, Miguel Comesaña-Hermo, Larousse Khosravi Khorashad, Ana Sousa-Castillo, Zhiming Wang, Moisés Pérez-Lorenzo, Tim Liedl, Alexander Govorov, Miguel Correa-Duarte

▶ **To cite this version:**

Yoel Negrín-Montecelo, Miguel Comesaña-Hermo, Larousse Khosravi Khorashad, Ana Sousa-Castillo, Zhiming Wang, et al.. Photophysical Effects behind the Efficiency of Hot Electron Injection in Plasmon-Assisted Catalysis: The Joint Role of Morphology and Composition. ACS Energy Letters, 2020, 5 (2), pp.395-402. 10.1021/acsenergylett.9b02478 . hal-02570541

HAL Id: hal-02570541
https://hal.science/hal-02570541

Submitted on 10 Nov 2020

HAL is a multi-disciplinary open access archive for the deposit and dissemination of scientific research documents, whether they are published or not. The documents may come from teaching and research institutions in France or abroad, or from public or private research centers.

L'archive ouverte pluridisciplinaire **HAL**, est destinée au dépôt et à la diffusion de documents scientifiques de niveau recherche, publiés ou non, émanant des établissements d'enseignement et de recherche français ou étrangers, des laboratoires publics ou privés.

Photophysical Effects behind the Efficiency of Hot Electron Injection in Plasmon-Assisted Catalysis: The Joint Role of Morphology and Composition

Yoel Negrín-Montecelo,[1] Miguel Comesaña-Hermo,[2,*] Larousse Khosravi Khorashad,[3] Ana Sousa-Castillo,[1] Zhiming Wang,[4] Moisés Pérez-Lorenzo,[1,*] Tim Liedl,[5] Alexander O. Govorov,[3,4,*] Miguel A. Correa-Duarte[1,*]

[1]Department of Physical Chemistry, Biomedical Research Center (CINBIO), Southern Galicia Institute of Health Research (IISGS), and Biomedical Research Networking Center for Mental Health (CIBERSAM), Universidade de Vigo, 36310 Vigo, Spain

[2]Université de Paris, ITODYS, CNRS, UMR 7086, 15 rue J-A de Baïf, F-75013 Paris, France

[3]Department of Physics and Astronomy, Ohio University, Athens, Ohio 45701, United States

[4]Institute of Fundamental and Frontier Sciences, University of Electronic Science and Technology of China, Chengdu, 610054, China

[5]Fakultät für Physik and Center for Nanoscience, Ludwig-Maximilians-Universität, Geschwister-Scholl-Platz 1, 80539 München, Germany

ABSTRACT

Plasmonic materials are intensively used in order to extend the photoactivity of large bandgap semiconductors into the visible light region. In this framework, the present study examines the joint role played by the morphology and composition of plasmonic nanoparticles in their photosensitizing capabilities. The critical influence of these parameters is evidenced by the effect of Au and core-shell Au@Ag nanorods on a TiO_2-driven photochemical probe reaction. In this case, the use of the bimetallic composites leads to a remarkable increase in the photocatalytic activity of the semiconductor compared to that found for the monometallic Au sensitizers. The mechanism behind this observation has then been computed theoretically concluding that, in terms of hot electron injection, the contribution of the transversal modes of the Au@Ag NRs together with the low damping of these nanostructures are responsible for the photocatalytic properties reported herein. The great potential of these architectures is confirmed by their notable performance toward photocatalytic hydrogen generation, rendering this approach an appealing strategy in the search of efficient solar-driven energy systems.

Noble metal nanoparticles (NPs) present outstanding optical properties given their strong interaction with light in the visible and NIR ranges of the electromagnetic spectrum.[1] This coupling arises due to the coherent oscillation of conduction electrons of the metallic objects in resonance with the incoming electromagnetic field, an effect known as localized surface plasmon resonance (LSPR).[2] As a result, a short-lived population of charge carriers ("hot" electrons) is created, being thermalized within the crystalline lattice of the metal on the femtosecond time scale.[3,4] Recent reports have shown that the combination of plasmonic objects with acceptor species such as organic molecules or semiconductors can lead to the exchange of charge carriers and hence to the possibility of using such species to drive chemical processes of interest.[5] Along these lines, plasmonic photosensitization has been identified as a promising interaction between a noble metal and a large bandgap semiconductor towards the formation of hybrid photocatalysts with improved efficiencies and broadband activity.[6,7] In this manner, the Schottky barrier created between both materials extends the lifetime of the hot carriers, thus leading to an accumulation of electrons at the conduction band of the semiconductor

and holes at the Fermi level of the metal that can be used in chemical processes such as water splitting, pollutant degradation or CO_2 reduction.[8] Two important parameters have to be mastered in order to achieve an efficient hot electron injection: formation of a physical interface and correct band alignment between the Fermi level of the metal and the conduction band of the semiconductor. Moreover, the extent of electromagnetic field enhancement at the interface has proven to play a major role in the density of hot electrons tunneling through the Schottky barrier, thus affecting the final activation of the acceptor.[9,10] All these parameters are strongly related with the chemical composition of the plasmonic entity. In this manner, a careful choice of the plasmonic material can lead to an enhanced electron injection and an overall improved photosensitization.

Even though Au is the most widely studied plasmonic metal, it is generally accepted that Ag colloids present higher electromagnetic field enhancement values and overall improved plasmonic responses, thus finding an important niche of applications in fields such as SERS spectroscopy or plasmonic sensing.[11] The main difference between both metals is related with the relative values of their respective interband transitions, intrinsic features of metals that can lead to non-radiative plasmonic damping and the loss of their unique optical properties.[11,12] In addition, Ag presents interband transitions of relatively high energy, hence blue-shifted with respect to the plasmon mode, reducing substantially any detrimental effect over the optical properties of these NPs. On the other hand, Au presents a relatively low energy threshold for the same type of transitions (2.5 vs. 3.8 eV in the case of Ag), leading therefore to a more prominent damping of the plasmon signal.

In order to evaluate the role played by the type of the plasmonic component in the hot electron injection mechanism and hence, in the overall photosensitization process, we have chosen Au NRs as the reference optical absorber. The multiple synthetic protocols available today account for an easy control over the dimensions and aspect ratio of these objects, thus ensuring a fine tuning of the longitudinal absorption band position in the visible and NIR ranges of the electromagnetic spectrum.[13] Interestingly, Au NRs can be used as templates for the growth of an homogeneous Ag shell, therefore allowing the formation of high quality Au@Ag NRs in which the thickness of the outermost metal can be also easily controlled.[14] Previous works have highlighted the synergistic effects stemming from this core@shell geometry, leading to the formation of

nanomaterials with improved properties in several catalytic and sensing applications.[15–18] Moreover, bimetallic Au-Ag nanostructures have shown enhanced performances for the generation of charged carriers when compared to their monometallic counterparts.[19–23] Following this approach, we have synthesized Au and Au@Ag NRs, in the latter case using small Au NRs as templates in order to obtain hybrid plasmonic resonators with very similar morphological features to those of the monometallic counterpart. Indeed, anisotropic NPs with very similar aspect ratios (2.1 and 2.3, respectively) are obtained (Figure 1a-f, see Supporting Information for details). The in-depth characterization of these plasmonic resonators has been previously described in the literature. These works pay special attention to their 3D atomic arrangement and the elucidation of their exposed facets.[14,24–26] Concerning the crystalline structure of monometallic single-crystalline Au NRs, it has been established that these objects hold an octagonal cross-section, thus exposing high-index {520} facets.[24,25] On the other hand, the reduction of Ag ions onto the preformed Au NRs induces a transformation of the original octagonal geometry toward the formation of a square prism that exposes {100} facets on the Ag shell (Figure S1).[14,26] Due to this morphological transition, the rounded corners observed in monometallic Au NRs transition to the formation of flat apexes in the bimetallic structures. It is also important to highlight that these morphologies have been chosen so that their respective longitudinal plasmon bands are centered at the same wavelength: 640 nm (Figure 1g). In the particular case of the Au@Ag NRs, the transversal hybrid mode (T-mode) is split in three signatures centered at 342, 400 and 475 nm, respectively.[27,28] These modes are clearly associated with the Ag shell, since the Au-based T-modes are typically less intense due to strong interband damping. Along these lines, the T2-mode (400 nm) is the Ag plasmon oscillation between the lower and upper parts of the Ag-shell. On the other hand, the T1-mode (342 nm) is the oscillation within the Ag shell between the two Ag surfaces (Figure 1k and S7). Moreover, there is also some hybridization of the modes between the Ag and Au components given the dynamic electric currents at ~400 nm supported by the latter. The third band centered at 475 nm may come from the polydispersity of the thickness of the Ag shell within the Au@Ag NRs. Although the theory does not provide the exact triplet structure of the blue peaks in the Au@Ag NRs (Figure 1h), it matches almost perfectly the intense T1 and T2-modes in the experimental Au@Ag spectrum (Figure S7).

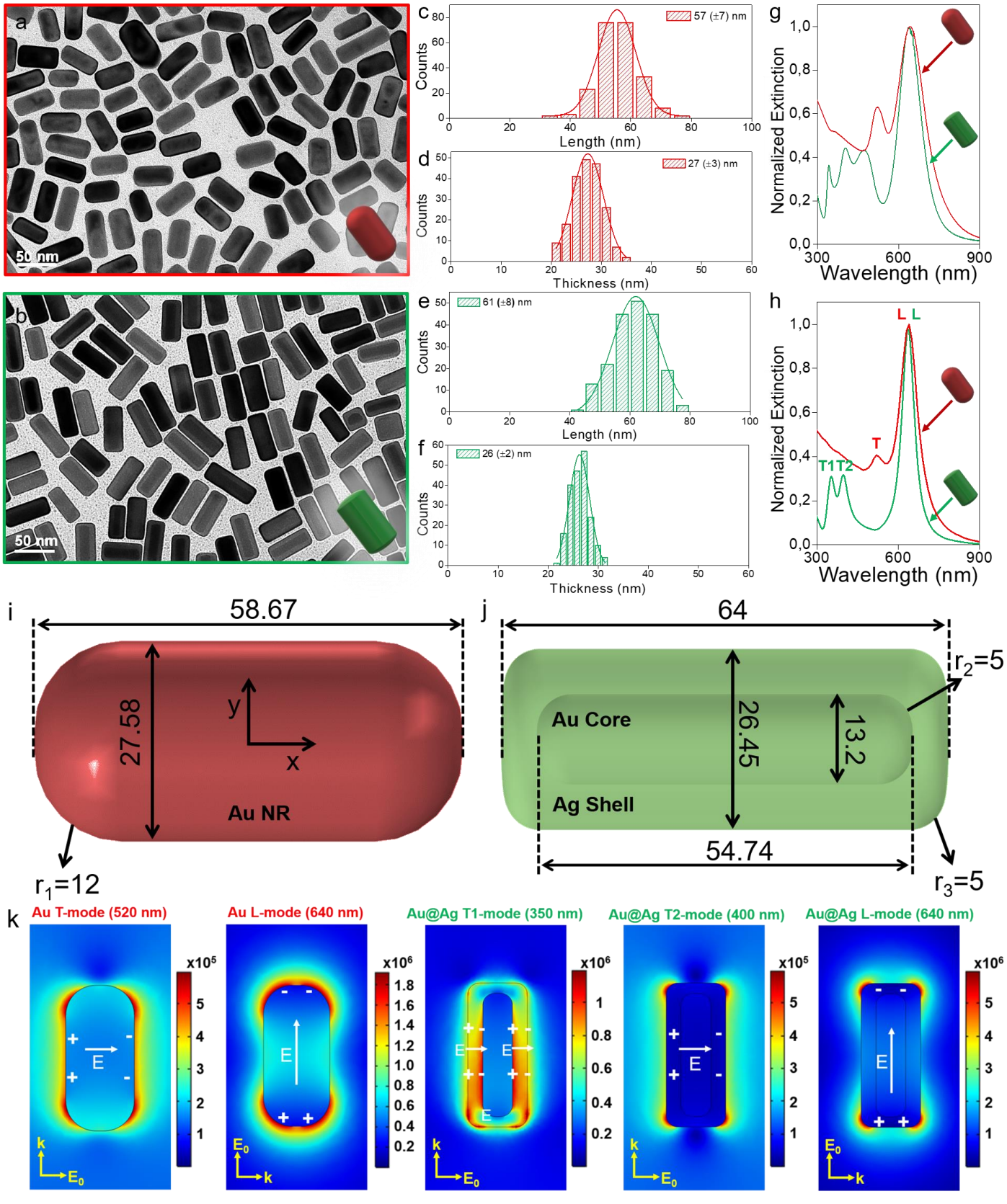

Figure 1. (a, b) TEM images, (c-f) size histograms, (g) experimental, and (h) theoretical extinction spectra of the Au NRs (red) and the Au@Ag NRs (green). Morphological features for the simulation of (i) Au NRs, and (j) Au@Ag NRs (being r_1, r_2 and r_3 the radii of curvature for rounding edges). (k) Near-field enhancement maps of the plasmonic modes of the Au and Au@Ag NRs.

Once the morphological and optical features of these plasmonic resonators are fully characterized, their capabilities as hot electron generators can be studied and comparisons between them can be inferred. In this way, the intrinsic singularities of the Ag coating in the framework of plasmonic photosensitization can be discussed. Consequently, we here implemented the different optical features of the monometallic and core@shell plasmonic NPs by integrating them into hybrid photocatalysts. As a result, the combination of Au and Au@Ag NRs with TiO_2 NPs leads to the perfect scenario in which the photosensitization of the latter can be directly correlated with the ability of the plasmonic component to generate hot carriers at the metal-semiconductor interface. Accordingly, hybrid nanocomposites have been obtained by taking advantage of the layer-by-layer assembly protocol, using electrostatic interactions as the main driving force (see the Supporting Information for details). With this aim, colloidal silica NPs with a diameter of 500 nm have been used as substrates for the deposition of TiO_2 NPs, leading to a homogeneous shell of 5 nm TiO_2 NPs (Figure 2a). In a subsequent step, the plasmonic component (either Au or Au@Ag NRs) is adsorbed, leading to the completion of the hybrid. This geometry ensures an easy control of the metal/TiO_2 ratio, a parameter of utmost importance in the photosensitization mechanism.[9] Moreover, the multilayer structures presented herein ensure a good interface between the active components, thus facilitating electron tunneling across this interface. In this manner, the controlled adsorption of different amounts of the given plasmonic component leads to the formation of a sandwich structure in which they are distributed over the entire surface of the substrate (Figure 2 and Figure S2 and S3). Interestingly, the optical properties of the final hybrids show the longitudinal plasmon band slightly red-shifted to 650 nm for both plasmonic materials. On the other hand, the transverse plasmon bands are hidden by the strong scattering contribution of the silica support (Figure S4).

The photocatalytic efficiency of the composites has been evaluated through the photodegradation of rhodamine B (RhB) as a model reaction, monitoring the decrease in absorbance of this dye as a function of time (Figure 2e, i) under irradiation with a solar simulator (λ: 350–2400 nm). It is important to remark that a partial photodegradation of RhB is observed in a reference sample formed by the functionalization of silica spheres with TiO_2 NPs alone (Figure S5). This residual degradation (12%) is the result of the direct photoexcitation of TiO_2 NPs with the small fraction of UV photons. On the other hand, the use of plasmonic NPs by themselves cannot account for the photodegradation of the aromatic dye (Figure S5). Subsequently, hybrid photocatalysts have been irradiated using different metal/TiO_2 ratios (0.05, 0.1 and 0.2) while keeping

constant the amount of semiconductor. In this setting, the use of monometallic Au NRs leads to a relatively poor degradation of the organic dye after 180 min, with a maximum of 32% for a metal/TiO_2 molar ratio of 0.1. Interestingly, when the same experiment is performed using a filter that blocks all excitation wavelengths below 400 nm, a very small decrease in the photodegradation of RhB is observed (25%, Figure S6). This result shows the minimal effect of the direct activation of TiO_2 compared to that of the plasmon-driven hot electron injection mechanism. Finally, the use of Au@Ag NRs leads to a quantitative degradation of the dye (99.4%) after the same irradiation time (Figure 2i), proving that the presence of an Ag shell on the Au NRs leads to an important improvement in the photoactivation of the semiconductor. Interestingly, when the amount of the plasmonic component is increased above a certain threshold (metal/TiO_2 molar ratio > 0.1 for both nanocomposites), a loss in the photocatalytic activity is observed. Such a detrimental effect has been previously explained as a consequence of a shorter lifetime of the excited electron-hole pairs, since metals can behave as recombination centers under specific conditions.[29] Moreover, given the particular geometry of the nanohybrids presented herein (the plasmonic objects are adsorbed onto the TiO_2 NPs) a reduction in the number of catalytic sites can take place, thus resulting in lower photocatalysis above a certain number of metal nanoparticles.

An additional probe reaction has been performed in order to ascertain the hot electron injection capabilities of the different plasmonic resonators. In this case, photocatalytic hydrogen generation assisted by formic acid has been followed using the hybrid nanomaterials as photocatalysts (Figure 2j). Interestingly, the core@shell NRs show an improved activity towards H_2 generation with respect to the monometallic NRs, confirming the results obtained for the photodegradation of the aromatic dye.

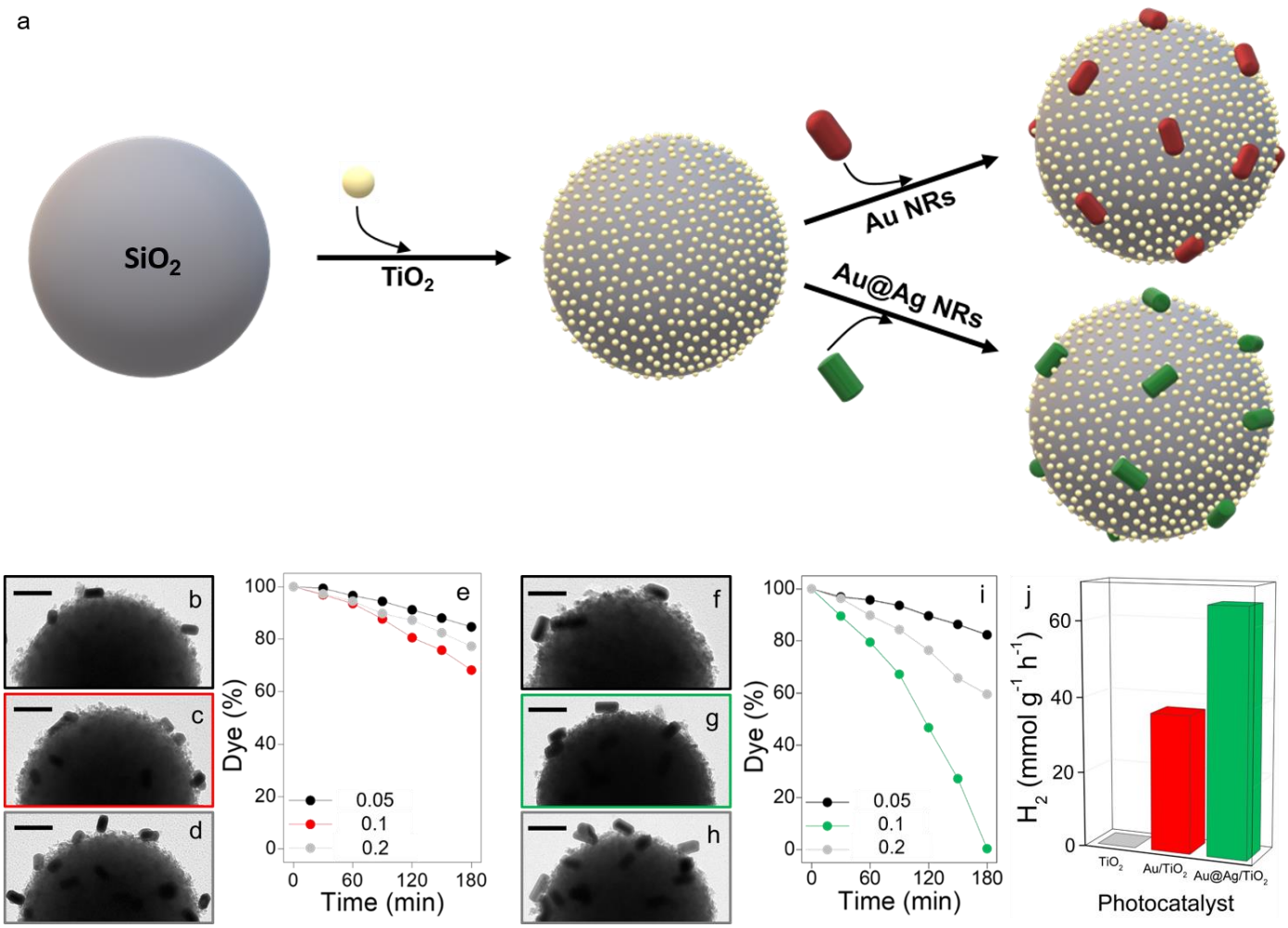

Figure 2. (a) Scheme depicting the layer-by-layer assembly of the hybrid photocatalysts. In a first stage, TiO_2 NPs are adsorbed onto 500 nm SiO_2 spheres. Subsequently, the chosen plasmonic component is added. (b-d) TEM images and (e) photocatalytic activity profiles of the hybrid photocatalysts formed with different amounts of Au NRs, leading to metal/TiO_2 molar ratios of: 0.05 (black); 0.1 (red) and 0.2 (grey). (f-h) TEM images and (i) photocatalytic activity profiles of the hybrid photocatalysts formed with different amounts of Au@Ag NRs, leading to metal/TiO_2 molar ratios of: 0.05 (black); 0.1 (green) and 0.2 (grey). (j) Photocatalytic hydrogen generation assisted by formic acid in the presence of SiO_2@TiO_2 (grey) and SiO_2@TiO_2 nanocomposites photosensitized by Au NRs (red) and Au@Ag NRs (green). Irradiation: 350–2400 nm; T=35 ^{O}C; P=1.0 atm; Metal/TiO_2=0.1 (where applicable). Scale bars in the TEM images are 100 nm.

Theoretical modeling has been performed in order to allow a correct interpretation of the optical and photochemical data obtained experimentally. In order to do so, two types of calculations have been performed using electromagnetic and quantum frameworks, respectively (Figure 3). With this aim, COMSOL software has been used to compute the optical features of both types of nanorods (mono- and bimetallic). The small morphological differences between the Au NRs and the Au@Ag NRs have been taken into consideration in the simulated extinction spectra of both structures, leading to theoretical values that match almost perfectly the experimental data (Figure 1h and Supporting Information). The appropriate dielectric constant of water for visible light (ε_{water} = 1.8) has been taken as matrix medium, while the dielectric constants of Au and Ag have been taken from the literature.[30] Geometrical parameters have been selected according to the data obtained from the TEM characterization of the individual NRs (Figure 1i, j). In particular, the lengths of the NRs have been chosen as: 59 nm in the case of Au and 64 nm for Au@Ag. Since the colloidal crystals are dispersed in solution, the calculated spectra are averaged over the three directions of light incidence, thus leading to spectra with both transverse and longitudinal plasmon peaks. Other essential parameters and information concerning the geometries of the NRs can be found in the Supporting Information.

Along with the classical electromagnetic calculations, the rates of generation of high-energy hot electrons have been computed using the quantum formalism developed in previous works.[10,31,32] This framework is used to calculate the surface-assisted generation of hot electrons, being particularly relevant to describe the injection of energetic electrons from a given plasmonic component onto the conduction band of a large bandgap semiconductor such as TiO_2 (Figure 3a, b). Therefore, the following equation has been used to compute the rates of hot-electrons transferred through the Schottky barrier:

$$Rate_{\text{high energy}} = \frac{1}{4}\frac{2}{\pi^2}\frac{e^2 E_F^2}{\hbar}\frac{(\hbar\omega - \Delta E_{\text{bar}})}{(\hbar\omega)^4}\int_S \left|E_{\omega,\text{normal}}\right|^2 ds \qquad (1)$$

Where $E_{\omega,normal}$ is the normal electric field inside a nanocrystal, which should be computed near the surface, E_F is the Fermi energy of the given metal and ΔE_{bar} = 1 eV is the Schottky barrier height for the NP-TiO_2 interface. The monochromatic rates presented in Figure 3a have been computed for a moderate light flux of 3.6×10^3 W/cm^2. Moreover, electronic parameters of Au and Ag such as the Fermi energies, can be found in a recent paper.[32]

Theoretical calculations have proven to be particularly valuable to understand the important difference in the photocatalytic behavior of the two types of plasmonic NRs. Firstly, the computed plasmonic signatures for the absorption and the hot-electron injection rates have been studied. Accordingly, given that the volumes of the computed NRs are very similar for both types of objects and Ag presents a plasmon-peak broadening that is a few times smaller than that of the one observed for Au, the Au@Ag NRs produce much stronger plasmonic resonances than the monometallic objects. Moreover, and in order to calculate the hot-electron rate at the plasmon resonance, a simple model consisting of a small spherical nanocrystal in which $Rate_{\text{at the plasmon peak}} \propto 1/\Gamma^2_{\text{plasmon}}$ (where Γ_{plasmon} is the width of the plasmon peak) can be used.[10,32] For gold and silver, Γ_{plasmon} is given by the Drude dissipation parameter, hence 0.078 and 0.020 eV, respectively. From the above numbers, one would expect a stronger plasmon peak for the generation of hot electrons in the Au@Ag NRs. Indeed, the core@shell NRs present a computed longitudinal plasmon-peak rate that is 2.6 times larger than that obtained for the monometallic Au NRs (Figure 3a).

Since the rates of the photocatalytic reaction have been measured for the broadband solar-like illumination using the spectral region above 350 nm, the monochromatic rate (1) should be integrated with the solar spectrum (with maximum excitation wavelength set at 1240 nm, that corresponds to the minimal photonic energy needed to excite an electron across the Schottky barrier). Hence:

$$Rate_{solar} = \int_{350nm}^{1240nm} d\lambda \times Rate_{\text{high energy}}(\lambda) \cdot I_{solar}(\lambda),$$
$$I_{solar}(\lambda) = \frac{A}{\lambda^5} \frac{1}{e^{\frac{hc}{\lambda \cdot kT_{sun}}} - 1}, \; T_{sun} = 5250K \qquad (2)$$

where the function $I_{solar}(\lambda)$ contains the black-body radiation spectrum at the temperature of the sun surface and A is a constant proportional to the total exciting flux. Since the integration starts at 350 nm (gray dotted line in Figure 3a), all the spectral features of the plasmonic objects within the integration interval have to be considered. In this manner, two prominent structures in the averaged-over-orientation spectra of the Au@Ag NRs are observed: a strong longitudinal plasmon resonance at 640 nm and a strong double-peak resonance centered at ~ 370 nm that corresponds to the hybrid transverse plasmonic resonances (green line in Figure 1h). Interestingly, the latter feature presents strong intensity while the transversal plasmon band of the Au NRs is damped due to interband transitions (Figure 1h). Accordingly, the nanocrystals coated with a Ag shell present a weak interband damping in the 370–400 nm interval, leading to strong plasmonic signatures. In this manner

the Au@Ag NRs presented herein hold transverse plasmons at ~370 nm that create an electromagnetic field concentrated in the Ag shell, thus avoiding plasmonic decay. Such a feature is an advantage of the Ag-based materials over monometallic Au nanocrystals, as can be observed in the computed absorption cross sections and rates of hot electron injection presented in Figure 1h and Figure 3a, respectively. Accordingly, the solar integral presented in (2) covers the two plasmonic structures of both types of NRs. Under these conditions an increase of the ratio between the solar rates for the Au and Au@Ag NRs is found to be 2.24.

The physical reasons behind the higher rates of hot-electron generation in the Au@Ag NRs as compared to the monometallic Au NRs can hence be ascribed to the relative importance of both plasmonic signatures (longitudinal and transverse). Firstly, the rate calculated following (2) is inversely proportional to the Drude broadening parameter,[10] hence leading to a more efficient formation of charge carriers in those nanorods with the sharper and stronger longitudinal plasmon bands. Moreover, the transverse signature in Au is strongly damped due to the interband transitions, whereas the hybrid transverse modes in the core@shell structure are very strong and active in the formation of charge carriers (Figure 3a). In order to prove experimentally the importance of the transversal plasmon modes of the Au@Ag NRs in the electron injection mechanism, the photodegradation tests have been repeated using a filter that blocks the excitation wavelengths below 500 nm, hence excluding the activity of the transversal modes of the bimetallic structures (Figure 3b). Interestingly, an important reduction in the photodegradation of RhB with respect to the broadband irradiation is observed (from to 99.4 to 50.9% after 180 min). This observation shows the important role that the hybrid transverse modes play in the photosensitization of the semiconductor in the Au@Ag structure. On the other hand, previous experiments with monometallic Au NRs have shown the null effect played by the tranverse plasmon signature in that case.[9]

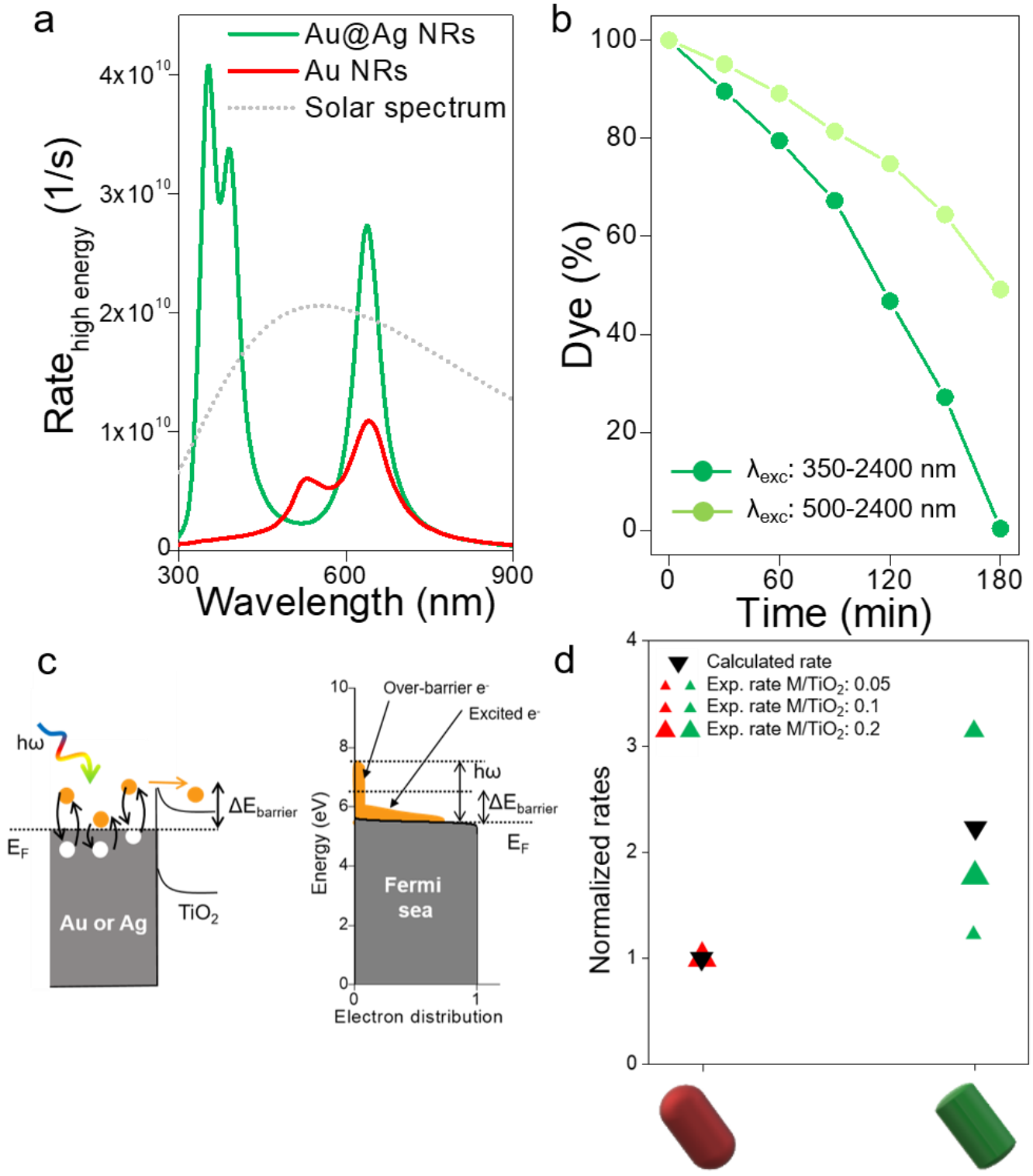

Figure 3. (a) Calculated rates of generation of hot electrons for the Au and Au-Ag NRs. (b) Photocatalytic activity profiles of the hybrid photocatalyst formed with Au@Ag NRs (metal/TiO_2 molar ratio of 0.1) using the entire spectrum of the solar simulator (dark green) and only the 500–2400 nm range (light green). (c) Schematic representation of the mechanism of hot-electron injection and the distribution of excited electrons in the optically-driven Fermi sea of electrons in a metal nanocrystal. (d) Comparison of the calculated hot-electron rates and the measured photocatalytic rates for the degradation of RhB. Note that the theoretical model can only take a single structure into account rendering ineffective the simulation of material ratios. All rates have been normalized with respect to the data obtained for monometallic Au NRs.

Finally, Figure 3d summarizes the calculated results and the experimental data obtained from the averaged photocatalytic reaction rates for the degradation of RhB presented in Figure 2. In order to compare both sets of data, the reaction rates of the two families of nanohybrids have been derived from the experiments following $Rate_{experimental} = \Delta(Dye\ \%)/\Delta t$, where the time interval is $\Delta t = 180$ min. For practical purposes, these rates have been normalized with respect to the values obtained for the monometallic Au NRs. Overall, semi-quantitative agreement is found between the calculated hot-electron rate and the experimental photocatalytic data. Such a result is reasonable taking into consideration the vast differences between the theoretical model that could not take into account the various ratios of materials and the complex photocatalytic reaction. While the former describes a simple framework in which the generation of high-energy electrons is calculated inside a given plasmonic object (Figure 3c), the photocatalytic degradation of a polycyclic molecule is a complex multi-step process in which reaction rates can be strongly influenced by experimental parameters.

In summary, we have investigated the role played by the nature of the plasmonic component in the photosensitization of TiO_2. We demonstrate that the use of bimetallic Au@Ag NRs ensures an improved photocatalytic activity with respect to monometallic Au NRs with similar geometries. Calculations show that the stronger plasmonic resonances and the limited interband damping effect in Ag ensure elevated hot-electron injection rates and hence, improved photosensitization of the semiconductor material. Accordingly, the present study demonstrates how the careful selection of the type and geometry of the plasmonic component can be used to engineer hybrid systems with enhanced optochemical capabilities, thus opening the door to their implementation in different areas of photocatalysis and photovoltaics such as environmental remediation, water splitting, CO_2 conversion, and organic solar cells.

ASSOCIATED CONTENT

The Supporting Information is available free of charge on the ACS Publications website at DOI: XXXX

Experimental methods; Theoretical modelling; TEM and HRTEM characterization; Optical characterization; Control Photocatalytic experiments; Unpolarized and polarized calculated spectra.

AUTHOR INFORMATION

Corresponding authors

*E-mail: miguel.comesana-hermo@u-paris.fr

*E-mail: moisespl@uvigo.es

*E-mail: govorov@helios.phy.ohiou.edu

*E-mail: macorrea@uvigo.es

ORCID

Yoel Negrín-Montecelo: 0000-0002-0977-7014

Miguel Comesaña-Hermo: 0000-0001-8471-5510

Larousse Khosravi Khorashad: 0000-0003-0461-5638

Ana Sousa-Castillo: 0000-0001-7811-0646

Moisés Pérez-Lorenzo: 0000-0002-7157-5966

Tim Liedl: 0000-0002-0040-0173

Alexander O. Govorov: 0000-0003-1316-6758

Miguel A. Correa-Duarte: 0000-0003-1950-1414

Notes

The authors declare no competing financial interest.

ACKNOWLEDGMENTS

The authors wish to thank Guillaume Wang (Université de Paris) for technical assistance with HRTEM. Y. N.-M., M. P.-L. and M. A. C.-D. acknowledge financial support from the Xunta de Galicia (Centro Singular de Investigación de Galicia, Acc. 2016-2019, ED431C 2016-034, IN607A 2018/5) and from the Spanish Ministerio de Economía y Competitividad under project CTM2017-84050-R. M. C.-H. has been funded by the CNRS Energy unit (Cellule Energie) through the project PEPS-CHEAP. Z. W. has been supported by National Basic Research Program of China (Project 2013CB933301) and National Natural Science Foundation of China (Project 51272038). T.L acknowledges funding by the cluster of excellence e-conversion. L. K. K. and A. O. G. are funded by the Volkswagen Foundation. A. O. G. has been supported via the 1000-talent Award of Sichuan and holds the Chang Jiang (Yangtze River) Chair Professorship in China.

REFERENCES

(1) Jain, P. K.; Huang, X.; El-Sayed, I. H.; El-Sayed, M. A. Noble Metals on the Nanoscale: Optical and Photothermal Properties and Some Applications in Imaging, Sensing, Biology, and Medicine. *Acc.*

Chem. Res. **2008**, *41*, 1578–1586.

(2) Mulvaney, P. Surface Plasmon Spectroscopy of Nanosized Metal Particles. *Langmuir* **1996**, *12*, 788–800.

(3) Saavedra, J. R. M.; Asenjo-Garcia, A.; García de Abajo, F. J. Hot-Electron Dynamics and Thermalization in Small Metallic Nanoparticles. *ACS Photonics* **2016**, *3*, 1637–1646.

(4) Liu, J. G.; Zhang, H.; Link, S.; Nordlander, P. Relaxation of Plasmon-Induced Hot Carriers. *ACS Photonics* **2017**, *5*, 2584–2595.

(5) Rao, V. G.; Aslam, U.; Linic, S. Chemical Requirement for Extracting Energetic Charge Carriers from Plasmonic Metal Nanoparticles to Perform Electron-Transfer Reactions. *J. Am. Chem. Soc.* **2018**, *141*, 643–647.

(6) Tatsuma, T.; Nishi, H.; Ishida, T. Plasmon-Induced Charge Separation: Chemistry and Wide Applications. *Chem. Sci.* **2017**, *8*, 3325–3337.

(7) Linic, S.; Christopher, P.; Ingram, D. B. Plasmonic-Metal Nanostructures for Efficient Conversion of Solar to Chemical Energy. *Nat. Mater.* **2011**, *10*, 911–921.

(8) Yu, Y.; Wijesekara, K. D.; Xi, X.; Willets, K. A. Quantifying Wavelength-Dependent Plasmonic Hot Carrier Energy Distributions at Metal/Semiconductor Interfaces. *ACS Nano* **2019**, *13*, 3629–3637.

(9) Sousa-Castillo, A.; Comesaña-Hermo, M.; Rodríguez-González, B.; Pérez-Lorenzo, M.; Wang, Z.; Kong, X.-T.; Govorov, A. O.; Correa-Duarte, M. A. Boosting Hot Electron-Driven Photocatalysis through Anisotropic Plasmonic Nanoparticles with Hot Spots in Au−TiO_2 Nanoarchitectures. *J. Phys. Chem. C* **2016**, *120*, 11690–11699.

(10) Kong, X.-T.; Wang, Z.; Govorov, A. O. Plasmonic Nanostars with Hot Spots for Efficient Generation of Hot Electrons under Solar Illumination. *Adv. Opt. Mater.* **2017**, *5*, 1600594.

(11) Rycenga, M.; Cobley, C. M.; Zeng, J.; Li, W.; Moran, C. H.; Zhang, Q.; Qin, D.; Xia, Y. Controlling the Synthesis and Assembly of Silver Nanostructures for Plasmonic Applications. *Chem. Rev.* **2011**, *111*, 3669–3712.

(12) Rycenga, M.; Hou, K. K.; Cobley, C. M.; Schwartz, A. G.; Camargo, P. H. C.; Xia, Y. Probing the Surface-Enhanced Raman Scattering Properties of Au–Ag Nanocages at Two Different Excitation Wavelengths. *Phys. Chem. Chem. Phys.* **2009**, *11*, 5903–5908.

(13) Scarabelli, L.; Sánchez-Iglesias, A.; Pérez-Juste, J.; Liz-Marzán, L. M. A "Tips and Tricks" Practical Guide to the Synthesis of Gold Nanorods. *J. Phys. Chem. Lett.* **2015**, *6*, 4270–4279.

(14) Gómez-Graña, S.; Goris, B.; Altantzis, T.; Fernández-López, C.; Carbó-Argibay, E.; Guerrero-Martínez, A.; Almora-Barrios, N.; López, N.; Pastoriza-Santos, I.; Pérez-Juste, J.; Bals, S.; Tendeloo, G. Van; Liz-Marzán, L. M. Au@Ag Nanoparticles: Halides Stabilize {100} Facets. *J. Phys. Chem. Lett.* **2013**, *4*, 2209–2216.

(15) Li, J. F.; Zhang, Y. J.; Ding, S. Y.; Panneerselvam, R.; Tian, Z. Q. Core-Shell Nanoparticle-Enhanced Raman Spectroscopy. *Chem. Rev.* **2017**, *117*, 5002–5069.

(16) Haldar, K. K.; Kundu, S.; Patra, A. Core-Size-Dependent Catalytic Properties of Bimetallic Au/Ag

Core-Shell Nanoparticles. *ACS Appl. Mater. Interfaces* **2014**, *6*, 21946–21953.

(17) Gómez-Graña, S.; Pérez-Juste, J.; Alvarez-Puebla, R. A.; Guerrero-Martínez, A.; Liz-Marzán, L. M. Self-Assembly of Au@Ag Nanorods Mediated by Gemini Surfactants for Highly Efficient SERS-Active Supercrystals. *Adv. Opt. Mater.* **2013**, *1*, 477–481.

(18) Samal, A. K.; Polavarapu, L.; Rodal-Cedeira, S.; Liz-Marzán, L. M.; Pérez-Juste, J.; Pastoriza-Santos, I. Size Tunable Au@Ag Core−Shell Nanoparticles: Synthesis and Surface-Enhanced Raman Scattering Properties. *Langmuir* **2013**, *29*, 15076–15082.

(19) Erwin, W. R.; Coppola, A.; Zarick, H. F.; Arora, P.; Miller, K. J.; Bardhan, R. Plasmon Enhanced Water Splitting Mediated by Hybrid Bimetallic Au-Ag Core-Shell Nanostructures. *Nanoscale* **2014**, *6*, 12626–12634.

(20) Valenti, M.; Venugopal, A.; Tordera, D.; Jonsson, M. P.; Biskos, G.; Schmidt-Ott, A.; Smith, W. A. Hot Carrier Generation and Extraction of Plasmonic Alloy Nanoparticles. *ACS Photonics* **2017**, *4*, 1146–1152.

(21) Misra, M.; Singh, N.; Gupta, R. K. Enhanced Visible-Light-Driven Photocatalytic Activity of Au@Ag Core-Shell Bimetallic Nanoparticles Immobilized on Electrospun TiO_2 Nanofibers for Degradation of Organic Compounds. *Catal. Sci. Technol.* **2017**, *7*, 570–580.

(22) Zhou, N.; Polavarapu, L.; Gao, N.; Pan, Y.; Yuan, P.; Wang, Q.; Xu, Q.-H. TiO_2 Coated Au/Ag Nanorods with Enhanced Photocatalytic Activity under Visible Light Irradiation. *Nanoscale* **2013**, *5*, 4236–4241.

(23) Yin, Z.; Wang, Y.; Song, C.; Zheng, L.; Ma, N.; Liu, X.; Li, S.; Lin, L.; Li, M.; Xu, Y.; Li, W.; Hu, G.; Fang, Z.; Ma, D. Hybrid Au-Ag Nanostructures for Enhanced Plasmon-Driven Catalytic Selective Hydrogenation through Visible Light Irradiation and Surface-Enhanced Raman Scattering. *J. Am. Chem. Soc.* **2018**, *140*, 864–867.

(24) Carbó-Argibay, E.; Rodríguez-González, B.; Gómez-Graña, S.; Guerrero-Martínez, A.; Pastoriza-Santos, I.; Pérez-Juste, J.; Liz-Marzán, L. M. The Crystalline Structure of Gold Nanorods Revisited: Evidence for Higher-Index Lateral Facets. *Angew. Chem. Int. Ed.* **2010**, *49*, 9397–9400.

(25) Goris, B.; Bals, S.; Van Den Broek, W.; Carbó-Argibay, E.; Gómez-Graña, S.; Liz-Marzán, L. M.; Van Tendeloo, G. Atomic-Scale Determination of Surface Facets in Gold Nanorods. *Nat. Mater.* **2012**, *11*, 930–935.

(26) Goris, B.; De Backer, A.; Van Aert, S.; Gómez-Graña, S.; Liz-Marzán, L. M.; Van Tendeloo, G.; Bals, S. Three-Dimensional Elemental Mapping at the Atomic Scale in Bimetallic Nanocrystals. *Nano Lett.* **2013**, *13*, 4236–4241.

(27) Cortie, M. B.; Liu, F.; Arnold, M. D.; Niidome, Y. Multimode Resonances in Silver Nanocuboids. *Langmuir* **2012**, *28*, 9103–9112.

(28) Jiang, R.; Chen, H.; Shao, L.; Li, Q.; Wang, J. Unraveling the Evolution and Nature of the Plasmons in (Au Core)-(Ag Shell) Nanorods. *Adv. Mater.* **2012**, *24*, OP200–OP207.

(29) Bumajdad, A.; Madkour, M. Understanding the Superior Photocatalytic Activity of Noble Metals

Modified Titania under UV and Visible Light Irradiation. *Phys. Chem. Chem. Phys.* **2014**, *16*, 7146–7158.

(30) Johnson, P. B.; Christy, R. W. Optical Constants of the Noble Metals. *Phys. Rev. B* **1972**, *6*, 4370–4379.

(31) Hartland, G. V.; Besteiro, L. V.; Johns, P.; Govorov, A. O. What's so Hot about Electrons in Metal Nanoparticles? *ACS Energy Lett.* **2017**, *2*, 1641–1653.

(32) Besteiro, L. V.; Kong, X.-T.; Wang, Z.; Hartland, G.; Govorov, A. O. Understanding Hot-Electron Generation and Plasmon Relaxation in Metal Nanocrystals: Quantum and Classical Mechanisms. *ACS Photonics* **2017**, *4*, 2759–2781.